# Accepted Manuscript

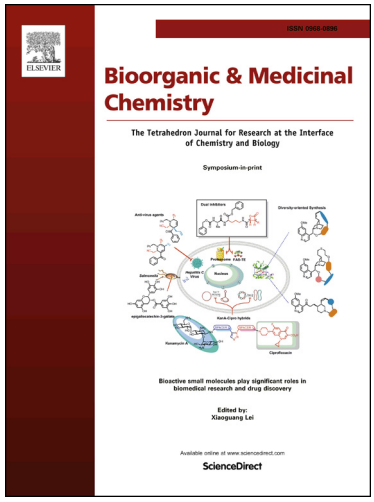


Synthesis, antiviral evaluation and molecular docking studies of $N^4$-aryl substituted/unsubstituted thiosemicarbazones derived from 1-indanones as potent anti-bovine viral diarrhea virus agents

María C. Soraires Santacruz, Matías Fabiani, Eliana F. Castro, Lucía V. Cavallaro, Liliana M. Finkielsztein

PII: S0968-0896(17)30432-7
DOI: http://dx.doi.org/10.1016/j.bmc.2017.05.056
Reference: BMC 13775

To appear in: *Bioorganic & Medicinal Chemistry*

Received Date: 2 March 2017
Revised Date: 22 May 2017
Accepted Date: 26 May 2017

Please cite this article as: Soraires Santacruz, M.C., Fabiani, M., Castro, E.F., Cavallaro, L.V., Finkielsztein, L.M., Synthesis, antiviral evaluation and molecular docking studies of $N^4$-aryl substituted/unsubstituted thiosemicarbazones derived from 1-indanones as potent anti-bovine viral diarrhea virus agents, *Bioorganic & Medicinal Chemistry* (2017), doi: http://dx.doi.org/10.1016/j.bmc.2017.05.056

# Synthesis, antiviral evaluation and molecular docking studies of $N^4$-aryl substituted/unsubstituted thiosemicarbazones derived from 1-indanones as potent anti-bovine viral diarrhea virus agents

María C. Soraires Santacruz[a,b,‡], Matías Fabiani[c,‡], Eliana F. Castro[c], Lucía V. Cavallaro[d,*], Liliana M. Finkielsztein[a,b,*].

[a] Cátedra de Química Medicinal, Departamento de Farmacología, Facultad de Farmacia y Bioquímica, Universidad de Buenos Aires, Junín 956, 1113, Ciudad Autónoma de Buenos Aires, Argentina

[b] Instituto de Química y Metabolismo del Fármaco (IQUIMEFA), Consejo Nacional de Investigaciones Científicas y Técnicas, Facultad de Farmacia y Bioquímica, Universidad de Buenos Aires, Junín 956, 1113, Ciudad Autónoma de Buenos Aires, Argentina

[c] Cátedra de Virología, Departamento de Microbiología, Inmunología y Biotecnología, Consejo Nacional de Investigaciones Científicas y Técnicas, Facultad de Farmacia y Bioquímica, Universidad de Buenos Aires, Junín 956, 1113, Ciudad Autónoma de Buenos Aires, Argentina

[d] Cátedra de Virología, Departamento de Microbiología, Inmunología y Biotecnología, Facultad de Farmacia y Bioquímica, Universidad de Buenos Aires, Junín 956, 1113, Ciudad Autónoma de Buenos Aires, Argentina.

* Corresponding authors. Tel: +541152874852, E-mail address: lfinkiel@ffyb.uba.ar (L. Finkielsztein) and Tel: +541152874474, E-mail address: lcavalla@ffyb.uba.ar (L. Cavallaro)

‡ These authors contributed equally to this paper

**Abstract**

A series of $N^4$-arylsubstituted thiosemicarbazones derived from 1-indanones and a set of compounds lacking such substitution in the $N^4$ position of the thiosemicarbazone moiety were synthesized and evaluated for their anti-bovine viral diarrhea virus (BVDV) activity. Among these, derivatives **2** and **15** displayed high activity ($EC_{50}$= 2.7 ± 0.4 and 0.7 ± 0.1 μM, respectively) as inhibitors of BVDV replication. Novel key structural features related to the anti-BVDV activity were identified by structure-activity relationship (SAR) analysis. In a previous study, the thiosemicarbazone of 5,6-dimethoxy-1-indanone (5,6-TSC) was characterized as a non-nucleoside inhibitor (NNI) of the BVDV RNA-dependent RNA polymerase. In the present work, cross-resistance assays were performed with the most active compounds. Such studies were carried out on 5,6-TSC resistant BVDV (BVDV-TSC$^r$ T1) carrying mutations in the viral polymerase. This BVDV mutant was also resistant to compound **15**. Molecular docking studies and MM/PBSA calculations were performed to assess the most active derivatives at the 5,6-TSC viral polymerase binding site. The differences in the interaction pattern and the binding affinity of derivative **15** either to the wild type or BVDV-TSC$^r$ T1 polymerase were key factors to define the mode of action of this compound.

**Keywords**

Thiosemicarbazones, Bovine viral diarrhea virus (BVDV), RNA-dependent RNA polymerase, Molecular docking, Antiviral activity, Antiviral resistance.

## 1. Introduction

Pestiviruses are the causative agents of serious infectious diseases in animals destined to human consumption. Such diseases are caused by the bovine viral diarrhea virus (BVDV) in bovines, the classical swine fever virus (CSFV) in swine, and the border disease virus (BDV) in sheep and goats. BVDV, which is one of the best characterized members of the *Pestivirus* genus, is an enveloped single-stranded positive polarity RNA virus. BVDV has a worldwide distribution and the percentages of persistently infected animals reaches 1-2% and a 60-80% present serum anti-BVDV antibodies.[1-3] In Argentina, the prevalence of anti-BVDV antibodies in adult cattle is roughly 70%.[4]

The economic losses caused by BVDV infections are associated with reduced milk production, lower conception rates, respiratory disorders and death during the acute infection. Fetal infection during early gestation stages may cause miscarriage, congenital defects, growth retardation, and may lead to the birth of persistently infected calves, which eventually develop a lethal mucosal disease.[5] Moreover, BVDV infections have a negative impact on the livestock reproductive performance.[6]

The prevention and control of these infections combine systemic vaccination and detection and removal of persistently infected animals. Vaccination programs are used extensively;[7] however, conventional vaccines (formulations with either attenuated or inactivated virus) may not be optimal for controlling BVDV infections.[8] Consequently, there is a need for effective and quick control tools; hence the use of antiviral agents may be useful for this purpose.

As the genome organization, translation, replication strategy and protein functions of pestiviruses closely resemble those of hepatitis C virus (HCV), the sole member of the *Hepacivirus* genus, BVDV, has also been adopted as a surrogate model for HCV studies.[9]

In a previous work, we synthesized a series of sixteen thiosemicarbazones (TSCs) derived from 1-indanones with different substitution patterns in the aromatic ring. These TSCs

were evaluated for their antiviral activity against BVDV by the viral cytopathic effect inhibition method.[10] The most potent compound was the TSC derived from 5,6-dimethoxy-1-indanone (5,6-TSC) (Fig. 1) ($EC_{50}$ = 1.8 ± 0.6 µM) with a selectivity index (SI) against BVDV of 80. It has been demonstrated that this compound acts by blocking the viral RNA synthesis both in cell culture and in isolated BVDV replication complexes.[11] Five independent populations of 5,6-TSC-resistant BVDV (BVDV-TSC$^r$; T1–5) (5,6-TSC $EC_{50}$ >80.0 µM) were selected. These populations carry an NS5B N264D mutation in the NS5B region of the viral genome encoding the BVDV RNA-dependent RNA polymerase (RdRp), whereas BVDV-TSC$^r$ T1 also bears an NS5B A392E mutation.[11]

Docking studies performed with the crystal structure of BVDV RdRp (PDB entry 1S48) and 5,6-TSC have shown significant differences between the wild type (wt) and the mutated form of the viral RdRp, both in terms of the amino acids involved in the interaction as well as the orientation of the ligand. These studies allowed concluding that 5,6-TSC is a non-nucleoside polymerase inhibitor (NNI) of BVDV.

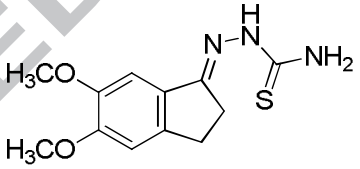


**Fig.1**. Thiosemicarbazone derived from 5,6-dimethoxy-1-indanone (5,6-TSC)

In previous studies, a series of $N^4$-arylsubstituted TSCs derived from 1-indanones ($N^4$-TSCs) were synthesized with the aim of improving the lipophilicity degree of TSCs.[12] In the present work, we investigated the anti-BVDV activity of a set of twelve $N^4$-TSCs derived from 1-indanones, six of which are not substituted and six, bear a 5,6-dimethoxy substitution in the indanic ring. Six of the twelve compounds are new derivatives. Moreover, four TSCs that did not bear any substitution in the $N^4$ position of the thiosemicarbazone moiety were also evaluated. The structural requirements for TSCs and

$N^4$-TSCs optimal activity are discussed. Furthermore, cross-resistance assays of the most active compounds against BVDV-TSC$^r$ T1 were performed. A molecular docking study was carried out to establish the differential interactions between wild type and mutated viral RdRp. Finally, molecular dynamics simulations were carried out to complement the experimental data of cross-resistance assays and to provide insights into the probable mode of action of the most active compounds.

## *2.* Materials and methods

### *2.1. Chemistry*

Melting points (uncorrected) were determined on a Thomas Hoover apparatus. Thin layer chromatography (TLC) was used to monitor reactions. IR spectra were recorded as KBr pellets using a Perkin Elmer Spectrum One FT-IR spectrophotometer. $^1$H and $^{13}$C NMR spectra were recorded on a Bruker 500 MHz spectrometer. High resolution mass spectra were acquired on Bruker micrOTOF-Q II spectrometer. 1-indanone, 5,6-dimethoxy-1-indanone, 4-fluorophenyl isothiocyanate, 4-nitrophenyl isothiocyanate, and 4-methoxyphenyl isothiocyanate were purchased from Sigma-Aldrich and used as received.

#### *2.1.1. General procedure for the synthesis of $N^4$-TSCs*

Method A: In the first step, a mixture of 1-indanone or 5,6-dimethoxy-1-indanone (3.8 mmol) and hydrazine hydrate 85% (0.9 mL) in isopropanol (5 mL) was heated under reflux for 1 h. After cooling, the solvent was evaporated and the residue was dissolved in $CH_2Cl_2$ (20 mL), dried over anhydrous $Na_2SO_4$ and evaporated again to render the crude derivative. Hydrazones were recrystallized from methanol. The physical parameters of the compounds obtained were in agreement with literature data.[13] In the second step, a solution of the corresponding isothiocyanate (3.0 mmol) in benzene (5 mL) was added dropwise to a solution of the hydrazone (2.5 mmol) in benzene (10 mL). The resulting

mixture was stirred at room temperature until the hydrazone was consumed. The hydrazone consumption was monitored by TLC. The solid obtained was filtered and washed with benzene (5 mL) and with ethanol (2 mL).

Method B: A mixture of 1-indanone or 5,6-dimethoxy-1-indanone (0.38 mmol), 85% hydrazine hydrate (21 µL), the corresponding isothiocyanate (0.43 mmol), acetic acid (20 µL) and isopropanol (0.5 mL) contained in a glass tube equipped with a screw cap and magnetic agitation was placed in a microwave synthesis reactor (Microwave 300 Anton Paar) at 90°C (30 W, 2.5 bar). Once the reaction was completed, as monitored by TLC, the obtained mixture was suspended in water (5 mL), filtered and washed with ethanol (2 mL). $N^4$-TSCs were recrystallized from ethanol.

*2.1.1.1. Indan-1-one N-(4-fluorophenyl)thiosemicarbazone (**8**).* Mp: 170-172°C. IR *v*/cm$^{-1}$ (KBr): 3279 (N-H), 3199 (N-H), 1606 (C=N), 1092 (C=S). $^1$H NMR ($CDCl_3$) *δ* ppm: 2.85 (m, 2H, $CH_2$), 3.22 (m, 2H, $CH_2$), 7.10 (m, 2H, H-Ar), 7.33 (t, *J*= 7.44 Hz, 1H, H-Ar), 7.38 (d, *J*= 7.59 Hz, 1H, H-Ar), 7.42 (t, *J*= 7.37 Hz, 1H, H-Ar), 7.62 (dd, *J*= 8.84, 4.81 Hz, 2H, H-Ar), 7.77(d, 7.72 Hz, 1H, H-Ar), 8.56 (s, 1H, NH), 9.26 (s, 1H, NH). $^{13}$C NMR ($CDCl_3$) *δ* ppm: 26.8, 28.7, 115.7, 115.8, 121.9, 125.9, 126.7, 126.7, 127.6, 131.6, 134.1, 136.8, 149.0, 157.4, 161.7, 176.6. HRMS (ESI) *m/z* $(M+H)^+$ calcd for $C_{16}H_{15}FN_3S$ 300.09652, found 300.09646.

*2.1.1.2. Indan-1-one N-(4-nitrophenyl)thiosemicarbazone (**9**).* Mp: 171-172°C. IR *v*/cm$^{-1}$ (KBr): 3362 (N-H), 3218 (N-H), 1597 (C=N), 1085 (C=S). $^1$H NMR ($CDCl_3$) *δ* ppm: 2.87 (m, 2H, $CH_2$), 3.24 (m, 2H, $CH_2$), 7.36 (t, *J*= 7.52 Hz, 1H, H-Ar), 7.40 (d, *J*= 7.62 Hz, 1H, H-Ar), 7.46 (t, *J*= 7.01 Hz, 1H, H-Ar), 7.80 (d, *J*= 7.71 Hz, 1H, H-Ar), 8.08 (d, *J*= 9.05Hz, 2H, H-Ar), 8.28(d, *J*= 9.08 Hz, 2H, H-Ar), 8.61 (s, 1H, NH), 9.71 (s, 1H, NH). $^{13}$C NMR ($CDCl_3$) *δ* ppm: 27.0, 28.7, 122.0, 122.4, 124.8, 126.0, 126.5, 127.7, 132.0, 136.5, 144.1, 144.5,

149.3, 158.2, 175.1. HRMS (ESI) *m/z* $(M+H)^+$ calcd for $C_{16}H_{15}N_4O_2S$ 327.09102, found 327.09136.

*2.1.1.3. Indan-1-one N-(4-methoxyphenyl)thiosemicarbazone (**10**).* Mp: 172-173 °C. IR *v*/$cm^{-1}$ (KBr): 3308 (N-H), 3210 (N-H), 1594 (C=N), 1091 (C=S). $^1H$ NMR ($CDCl_3$) $\delta$ ppm: 2.83 (m, 2H, $CH_2$), 3.21 (m, 2H, $CH_2$), 3.83 (s, 3H, $OCH_3$), 6.94 (d, *J*= 8.21 Hz, 2H, H-Ar), 7.32 (t, *J*= 7.21 Hz, 1H, H-Ar), 7.38 (d, *J*= 7.58 Hz, 1H, H-Ar), 7.41 (t, *J*= 7.66 Hz, 1H, H-Ar), 7.53 (d, *J*= 8.13 Hz, 2H, H-Ar), 7.77 (d, 7.42 Hz, 1H, H-Ar), 8.47 (s, 1H, NH), 9.20 (s, 1H, NH). $^{13}C$ NMR ($CDCl_3$) $\delta$ ppm: 26.7, 28.7, 55.6, 114.2, 121.9, 125.9, 126.6, 126.7, 127.5, 131.1, 131.4, 137.0, 148.9, 156.9, 157.0, 158.1, 176.8. HRMS (ESI) *m/z* $(M+H)^+$ calcd for $C_{17}H_{18}N_3OS$ 312.11651, found 312.11651.

*2.1.1.4. 5,6-Dimethoxyindan-1-one N-(4-fluorophenyl)thiosemicarbazone (**14**).* Mp: 185-186 °C. IR *v*/$cm^{-1}$ (KBr): 3300 (N-H), 3196 (N-H), 1605 (C=N), 1078 (C=S). $^1H$ NMR ($CDCl_3$) $\delta$ ppm: 2.86 (m, 2H, $CH_2$), 3.15 (m, 2H, $CH_2$), 3.95 (s, 3H, $OCH_3$), 3.96 (s, 3H, $OCH_3$), 6.85 (s, 1H, H-Ar), 7.12 (dd, *J*= 8.61, 8.52 Hz, 2H, H-Ar), 7.18 (s, 1H, H-Ar), 7.61 (dd, *J*= 8.76, 4.83 Hz, 2H, H-Ar), 8.52 (s, 1H, NH), 9.19 (s, 1H, NH). $^{13}C$ NMR (DMSO-$d_6$) $\delta$ ppm: 28.41, 28.58, 56.10, 56.28, 104.9, 108.3, 115.2, 128.8, 129.9, 136.2, 143.0, 149.3, 152.6, 159.0, 160.2, 177.0. HRMS (ESI) *m/z* $(M+H)^+$ calcd for $C_{18}H_{19}FN_3O_2S$ 360.11765, found 360.11645.

*2.1.1.5. 5,6-Dimethoxyindan-1-one N-(4-nitrophenyl)thiosemicarbazone (**15**).* Mp: 214-216 °C. IR *v*/$cm^{-1}$ (KBr): 3273 (N-H), 3191 (N-H), 1598 (C=N), 1075 (C=S). $^1H$ NMR ($CDCl_3$) $\delta$ ppm: 2.86 (m, 2H, $CH_2$), 3.14 (m, 2H, $CH_2$), 3.94 (s, 3H, $OCH_3$), 3.96 (s, 3H, $OCH_3$), 6.84 (s, 1H, H-Ar), 7.16 (s, 1H, H-Ar), 8.04 (d, *J*= 8.93 Hz, 2H, H-Ar), 8.26 (d, *J*= 8.93 Hz, 2H, H-Ar), 8.56 (s, 1H, NH), 9.58 (s, 1H, NH). $^{13}C$ NMR (DMSO-$d_6$) $\delta$ ppm: 28.6, 28.7, 56.1,

56.3, 105.1, 108.3, 112.9, 124.7, 126.9, 129.5, 143.7, 146.1, 149.3, 152.9, 160.6, 175.7. HRMS (ESI) *m/z* $(M+H)^+$ calcd for $C_{18}H_{19}N_4O_4S$ 387.11215, found 387.11081.

*2.1.1.6. 5,6-Dimethoxyindan-1-one N-(4-methoxyphenyl)thiosemicarbazone (**16**).* Mp: 198-199 ºC. IR *v*/$cm^{-1}$ (KBr): 3312 (N-H), 3216 (N-H), 1603 (C=N), 1075 (C=S). $^1H$ NMR ($CDCl_3$) *δ* ppm: 2.82 (m, 2H, $CH_2$), 3.12 (m, 2H, $CH_2$), 3.82 (s, 3H, $OCH_3$), 3.92 (s, 3H, $OCH_3$), 3.93 (s, 3H, $OCH_3$), 6.83 (s, 1H, H-Ar), 6.93 (d, *J*= 9.00 Hz, 2H, H-Ar), 7.15 (s, 1H, H-Ar), 7.49 (d, *J*= 8.70 Hz, 2H, H-Ar), 8.47 (s, 1H, NH), 9.11 (s, 1H, NH). $^{13}C$ NMR (DMSO-$d_6$) *δ* ppm: 28.3, 28.6, 55.8, 56.1, 56.3, 104.9, 108.3, 113.8, 128.3, 130.0, 132.7, 142.9, 149.3, 152.5, 157.5, 158.6, 177.1. HRMS (ESI) *m/z* $(M+H)^+$ calcd for $C_{19}H_{22}N_3O_3S$ 372.13764, found 372.13836.

*2.2. Biology*

*2.2.1. Cells and viruses*

Madin Darby bovine kidney cells (MDBK NBL-1; ATCC CCL-22) were grown in Eagle's Minimal Essential Medium (E-MEM), supplemented with 10% γ-irradiated fetal bovine serum (FBS, *Internegocios*), 2 mM L-glutamine, 100 µM nonessential amino acids (Gibco), 100 µg/mL streptomycin, and 100 IU/mL penicillin (Growing medium, GM). Bovine viral diarrhea virus (BVDV) type 1 NADL strain, cytopathic biotype (BVDV-1, ATCC VR 534) was provided by Dr. Laura Weber, INTA Castelar, Buenos Aires, Argentina. The 5,6-TSC-resistant BVDV (BVDV-$TSC^r$ T1) carrying both N264D and A392E mutations in the NS5B region had previously been selected in our laboratory.[11]

*2.2.2. Compounds*

All compounds were diluted in dimethyl sulfoxide at 5 or 1 mg/ml immediately before use. Further serial dilutions were made in Infection Medium (IM) (E-MEM, supplemented with

2.5% donor horse serum-DHS, Gibco, 2 mM L-glutamine, 100 µM nonessential amino acids, 100 µg/mL streptomycin and 100 IU/mL penicillin).

*2.2.3. Cytotoxicity assay*

MDBK cells were resuspended in GM and seeded at a density of 1x $10^4$ cells per well in a 96-well cell culture plate. After 24 h of incubation at 37°C, 5% $CO_2$, GM was removed and serial dilutions of the test compounds were added. Mock-treated cells were included as control (MT). Cells were allowed to proliferate for 3 days at 37°C and then cell viability was estimated by the MTS/PES method (Cell Titer 96 $Aq_{ueous}$ One Solution Cell Proliferation Assay, Promega), following the manufacturer´s instructions. After incubating for 2.5 h at 37°C, the absorbance values were determined at 490 nm, which is directly proportional to the number of viable cells. The cell viability percentage was calculated as follows: Cell viability (%) = $Abs_{TSC}$ x 100/ $Abs_{MT.}$ The cytotoxic concentration 50% ($CC_{50}$) was defined as the compound concentration that inhibited the proliferation of exponentially growing cells by 50% and calculated from dose-response curves using GraphPad Prism version 5.00 for Windows. Three independent experiments were carried out in quadruplicate.

*2.2.4. Plaque reduction assay for BVDV*

MDBK cells were resuspended in GM and seeded at a density of 1.3 x$10^5$ cells per well in a 24-well culture plate. After incubating for 24 h in a 5% $CO_2$ incubator at 37°C, GM was removed, cells were washed with Phosphate buffer saline (PBS) and then infected with 100 plaque-forming units (PFU) of BVDV. After 1 h of incubation at 37 ºC, the inoculum was removed and cell monolayers were washed twice with PBS. After washing, 0.2 ml of serial dilutions (1:2) of each compound in IM and 0.8 ml of overlay medium (IM supplemented with 1% methylcellulose) were added to each well. Mock-infected cells with and without compound and infected cells without compound (infected untreated control -

UTC), were included as controls. After incubating for 72 h at 37°C with 5% $CO_2$, cells were fixed with 10% formalin, stained with 0.75% crystal violet and the viral plaques counted. The reduction of plaques (%) at each compound concentration (TSCx) was calculated as [1-(no. plaques $_{TSCx}$/no. plaques $_{UTC}$)] x 100. The effective concentration 50% ($EC_{50}$) was defined as the compound concentration that caused a reduction in the number of viral plaques by 50% with respect to the UTC and was determined from dose-response curves using GraphPad Prism version 5.00 for Windows. Three independent experiments were carried out in triplicate. Finally, the selectivity index (SI) was calculated as $CC_{50}/EC_{50}$.

*2.2.5. Cytopathic effect reduction assay*

MDBK cells were resuspended in GM and seeded at a density of 1 x $10^4$ cells per well in a 96-well culture plate. After incubating for 24 h in a 5% $CO_2$ incubator at 37°C, cells were infected with BVDV at a multiplicity of infection (MOI) of 0.01 PFU/cell. Serial dilutions of each TSC were tested in quadruplicate. Mock-infected cells (MI) and infected cells without compound (UTC) were included as controls. After incubating for 72 h at 37°C, the cytopathic effect was determined by measuring cell viability by the MTS/PES method (Cell Titer 96 $Aq_{ueous}$ One Solution Cell Proliferation Assay, Promega) as described above. The reduction of viral cytopathic effect (CPE) was calculated as follows: CPE reduction (%) = ($Abs_{TSCx}$ –$Abs_{UTC}$) X100 / ($Abs_{MI}$ – $Abs_{UTC}$). The $EC_{50}$ was defined as the concentration of compound that reduced the CPE by 50% and was calculated from dose-response curves using GraphPad Prism version 5.00 for Windows. Two independent experiments were performed in quadruplicate.

*2.2.6. Time-of-drug-addition study: effect on viral replication*

MDBK cells were resuspended in GM and seeded at a density of 1x$10^4$ cells per well in a 96-well culture plate. After incubating for 24 h in a 5% $CO_2$ incubator at 37°C, cells were

precooled for 30 min on ice and then infected with BVDV (MOI = 1). After 90 min of adsorption on ice, the inoculum was removed, and monolayers were washed twice with PBS and incubated in IM. At different time points post-infection (p.i.), a 25 µM solution of compound **2** (10 x $EC_{50}$) was added. This procedure was repeated up to 12 h p.i. After incubating for 48 h at 37°C, the CPE was determined by measuring cell viability by the MTS/PES method (Cell Titer 96 Aqueous One Solution Cell Proliferation Assay, Promega) as described above. Mock-infected and infected cells without compound were added as controls. Three independent experiments were carried out in quadruplicate.

*2.3. Molecular docking study*

Docking studies were carried out using Autodock 4.2 program[14] for 5,6-TSC and the more potent compounds **2** and **15**. To this end, the X-ray structure of the RdRp of BVDV was obtained from Protein Data Bank (http://www.rcsb.org) (PDB entry 1S48). Selenomethionine residues were modified back to methionine residues, polar hydrogens were added and the water molecules were removed. The enzyme molecule was optimized with NAMD 2.9 software[15] using the CHARMM force field in order to minimize crystallographic-induced bond clashes. The 3D structures of the compounds were constructed using HyperChem 8.0.7 software and were pre-optimized with the MM+ procedure. The resulting geometries were refined by means of the AM1 semi-empirical method. A full geometry optimization of minimum energy conformations was subsequently carried out at the HF/6-31G(d) *ab initio* level using Gaussian 09. The ligand files were prepared in pdbqt format using Autodock Tools 1.5.6. The putative binding site for the selected compounds on the BVDV RdRp was determined using the metapocket 2.0 server.[16] By this procedure, three putative binding sites on the surface of the enzyme were found; however, only one was located in the region where mutations of RdRp had been observed. Hence, this site was chosen to carry out the molecular docking procedure. An

affinity grid with a dimension of 60 x 60 x 60 points in the xyz plane and a 0.375 Å spacing was generated with the AutoGrid and centered on the chosen site. Ligands were fully flexible during the procedure whereas the protein remained rigid. The docking was carried out with 1000 runs using the Lamarckian genetic algorithm (LGA). The final selection of binding mode was made according to the estimated free binding energy and size of clusters. The binding interactions were visualized by the Chimera 1.8 software.[17]

*2.4. MD simulations and binding free energy calculation*

Best docked poses were used as the starting structures for molecular dynamics (MD). Simulations were performed with NAMD 2.9 software using CHARMM36 and CHARMM general force field to represent the protein-ligand systems.[18,19] Each complex was solvated in a cubic TIP3P water[20] with the minimal distance of 10 Å from the protein surface to the edge of the box and chlorine atoms were added in order to neutralize the system. Energy minimizations were performed with the protein being restrained, followed by second energy minimization without restrain. The temperature was gradually increased to 300 K during 300 ps using a NVT ensemble and then equilibrated over a period of 3 ns at the reference pressure of 1 atm and a temperature of 300 K. The MD productions were carried out for 6 ns under NPT conditions and an integration time step of 2 fs. The particle mesh Ewald (PME) was used to treat long-range electrostatics interactions;[21] the SHAKE algorithm[22] was applied to all hydrogen atoms and the van der Waals cutoff was set to 10 Å. The simulations trajectories were analyzed using VMD.[23]

The binding free energies ($\Delta G_{bind}$) were estimated via the widely used Molecular Mechanic/Poisson Boltzmann Surface Area (MM/PBSA) method.[24-27] According to this approach, the free energy was calculated for each ligand/protein system as described by the following equations:

$$\Delta G_{bind} = G_{complex} - (G_{protein} + G_{ligand}) = \Delta H_{bind} - T\Delta S_{bind}$$

$$\Delta H_{bind} = \Delta E_{MM} + \Delta G_{PB} + \Delta G_{NP}$$

where $\Delta E_{MM}$ describes the molecular mechanical energies, $\Delta G_{PB}$ and $\Delta G_{NP}$ define the polar and non-polar solvation energy, respectively. The entropic contribution was obtained by performing normal mode analysis in order to be able to calculate the total $\Delta G$.

## 3. Results and Discussion

### *3.1. Synthesis*

TSCs **1**-**4** (Table 1)[12] were synthesized with high yield from the corresponding 1-indanones treated with thiosemicarbazide, according to the general procedure described previously.[10] $N^4$-TSCs **5**-**16** were obtained through two different synthetic methodologies.[12] The first approach (Method A, Scheme 1) involved a procedure comprising two steps: (1) synthesis of hydrazone from the corresponding 1-indanone and hydrazine hydrate, (2) preparation of the desired $N^4$-TSCs by reaction of hydrazone with the suitable isothiocyanate. The second one (Method B, Scheme 1) was a one-pot multicomponent coupling reaction method performed under microwave irradiation (MW). The second route afforded $N^4$-TSCs in short reaction times (hours for Method A and minutes for Method B). Comparative results obtained in both synthetic processes for new derivatives (**8**-**10** and **14**-**16**) are shown in Table 2. The yields were higher when $N^4$-TSCs were prepared by Method B, except for compound **10**. The structure of new compounds was confirmed by $^1$H- and $^{13}$C-NMR, IR and HRMS data. The general structure of the TSCs and $N^4$-TSCs studied is shown in Table 1.

**Table 1**. Synthesized TSCs and $N^4$-TSCs

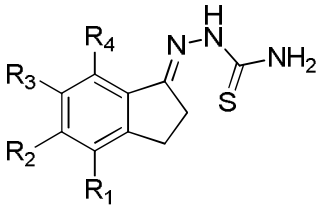

**1-4**

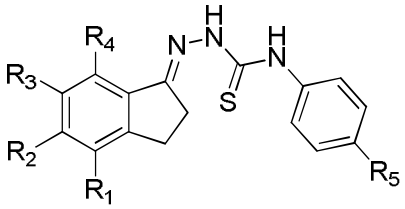

**5-16**

| Compound | $R_1$ | $R_2$ | $R_3$ | $R_4$ | $R_5$ |
|---|---|---|---|---|---|
| **1** | $NO_2$ | H | H | H | - |
| **2** | H | H | $NO_2$ | H | - |
| **3** | H | F | H | H | - |
| **4** | $CH_3$ | Br | H | $CH_3$ | - |
| **5** | H | H | H | H | H |
| **6** | H | H | H | H | $CH_3$ |
| **7** | H | H | H | H | Cl |
| **8** | H | H | H | H | F |
| **9** | H | H | H | H | $NO_2$ |
| **10** | H | H | H | H | $OCH_3$ |
| **11** | H | $OCH_3$ | $OCH_3$ | H | H |
| **12** | H | $OCH_3$ | $OCH_3$ | H | $CH_3$ |
| **13** | H | $OCH_3$ | $OCH_3$ | H | Cl |
| **14** | H | $OCH_3$ | $OCH_3$ | H | F |
| **15** | H | $OCH_3$ | $OCH_3$ | H | $NO_2$ |
| **16** | H | $OCH_3$ | $OCH_3$ | H | $OCH_3$ |

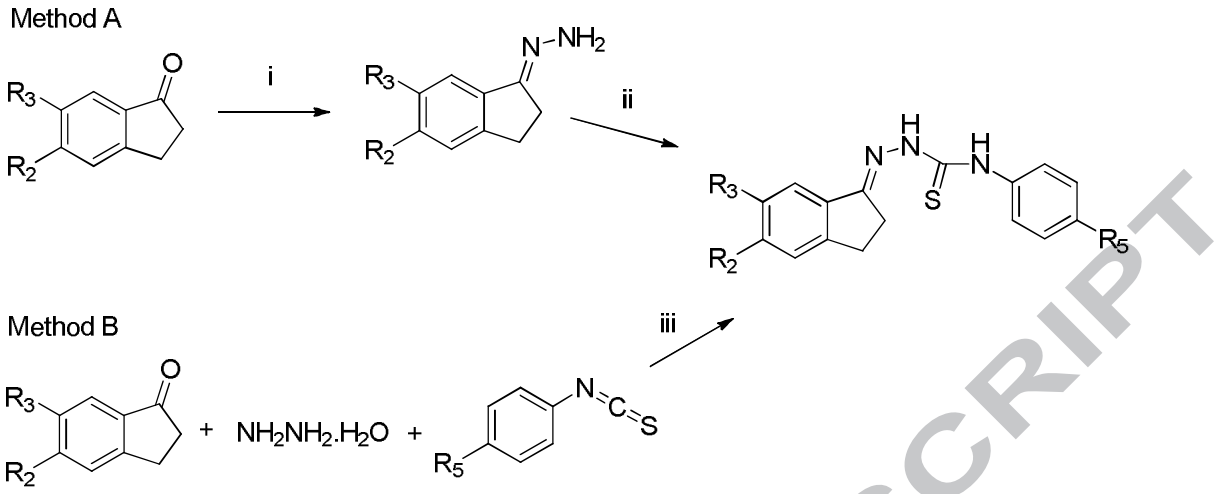


**Scheme 1**. Synthetic routes for the obtention of $N^4$-TSCs. Reaction conditions: (i) 85% hydrazine hydrate/isopropanol, reflux; (ii) isothiocyanate/benzene, room temperature; (iii) acetic acid, isopropanol, MW.

**Table 2**. Comparative results obtained in the synthesis of $N^4$-TSCs by Methods A and B

| $N^4$-TSCs | $R_1$ | $R_2$ | $R_3$ | $R_4$ | $R_5$ | Method A | | Method B | |
|---|---|---|---|---|---|---|---|---|---|
| | | | | | | Time (h) | Yield (%) | Time (min) | Yield (%) |
| **8** | H | H | H | H | F | 27 | 19 | 130 | 87 |
| **9** | H | H | H | H | $NO_2$ | 20 | 46 | 45 | 70 |
| **10** | H | H | H | H | $OCH_3$ | 72 | 86 | 60 | 69 |
| **14** | H | $OCH_3$ | $OCH_3$ | H | F | 96 | 41 | 30 | 53 |
| **15** | H | $OCH_3$ | $OCH_3$ | H | $NO_2$ | 72 | 56 | 65 | 100 |
| **16** | H | $OCH_3$ | $OCH_3$ | H | $OCH_3$ | 73 | 29 | 45 | 52 |

*3.2. Antiviral activity*

The antiviral activity exerted by compounds **1**–**16** against BVDV was evaluated by the plaque-forming units (PFU) reduction assay and the results are shown in Table 3. Reference compounds 5,6-TSC and Ribavirin were also included.

The TSC derived from 6-nitro-1-indanone (**2**) was the most active compound among the

non-substituted TSCs evaluated (**1**-**4**), with an anti-BVDV activity ($EC_{50}$= 2.7 ± 0.4 µM) that was similar to that of 5,6-TSC ($EC_{50}$= 3.8 ± 0.4 µM).

Among the twelve $N^4$-TSCs evaluated (**5**-**16**), those derived from the 1-indanone (**5**-**10**) exerted a PFU reduction from 15 to 40% at the highest concentrations tested ($EC_{50}$>10 µM or $EC_{50}$>20 µM). Derivatives obtained from 5,6-dimethoxy-1-indanone (**11-16**) were the most active ones, with $EC_{50}$ values ranging from 0.7 to 12.9 µM. Compound **15** was the most potent of the $N^4$-TSCs series, with an $EC_{50}$ value that was almost 6-fold lower than that of 5,6-TSC ($EC_{50}$= 0.7 ± 0.1 µM and 3.8 ± 0.4 µM, respectively). None of the $N^4$-TSCs showed significant cytotoxicity at the concentrations evaluated.

For several compounds, $CC_{50}$ values could not be determined due to the reduced solubility in infection medium.

**Table 3.** *In vitro* anti-BVDV activity and cytotoxicity of TSCs and $N^4$-TSCs derivatives

| Compound | $EC_{50}$[a] (μM) | $CC_{50}$[a] (μM) | S.I.[b] |
|---|---|---|---|
| **1** | 6.1 ± 0.6 | 84.6 ± 5.4 | 14.2 |
| **2** | 2.7 ± 0.4 | >25 | >9.3 |
| **3** | 9.0 ± 0.1 | 41.9 ± 5.6 | 5.4 |
| **4** | 7.4 ± 0.4 | >100 | >13.5 |
| **5** | >10 | >10 | - |
| **6** | >20 | >20 | - |
| **7** | >20 | >20 | - |
| **8** | >20 | >20 | - |
| **9** | >10 | >10 | - |
| **10** | >10 | >10 | - |
| **11** | 8.4 ± 0.4 | >10 | >1.2 |
| **12** | 8.8 ± 0.1 | >20 | >2.3 |
| **13** | 6.6 ± 0.2 | >10 | >1.5 |
| **14** | 4.0 ± 0.8 | >20 | >5.0 |
| **15** | 0.7 ± 0.1 | >10 | >14.3 |
| **16** | 12.9 ± 0.9 | >20 | >1.6 |
| **5,6-TSC** | 3.8 ± 0.4 | >80 | >21.1 |
| **Ribavirin** | 7.7 ± 1.5 | 54.4 ± 3.8 | 7.1 |

$EC_{50}$= Concentration of compound that reduces the number of PFU by 50% with respect to the untreated viral control. $CC_{50}$= Concentration of compound that inhibits cell viability by 50% with respect to the untreated cell control. [a] Data are expressed as mean values ± SD from at least 3 independent experiments. [b] *In vitro* selectivity index ($CC_{50}/EC_{50}$).

*3.3. Structure-activity relationship*

In our previous work neither 4 nor 6 indanic ring monosubstituted TSCs were assessed.[10] Interestingly, the introduction of a nitro group in these positions led to the generation of the most active compounds (**1** and **2,** respectively). The TSC bearing a fluorine atom at position 5 was moderately active against BVDV, but it was less active than the bromine and chlorine analogs reported previously.[10] Finally, among TSCs, compound **4** showed an

activity that was similar to that of other trisubstituted compounds with different pattern of methyl and halogen substituents.[10]

In the group of $N^4$-TSCs, it was clear that the presence of the methoxy groups in the nucleus was essential for the anti-BVDV activity. None of the $N^4$-TSCs derived from 1-indanone were active (**5**-**10**), whereas all $N^4$-TSCs derived from 5,6-dimethoxy-1-indanone exhibited anti-BVDV activity (**11**-**16**). Among $N^4$-TSCs **11**-**16**, the nature of the substituent at position $R_5$ played an important role in the anti-BVDV activity. Thus, the introduction of electron-donating substituents in the phenyl substituent such as the methyl (**12**) ($EC_{50}$= 8.8 ± 0.1 µM) or the methoxyl group (**16**) ($EC_{50}$= 12.9 ± 0.9 µM) generated analogs with similar or reduced antiviral activity compared to compound **11** ($R_5$= H) ($EC_{50}$= 8.4 ± 0.4 µM). Conversely, the presence of electron-withdrawing substituents at $R_5$ resulted in $N^4$-TSCs with high anti-BVDV activity. Thus, the incorporation of a halogen atom led to improved antiviral activity. In particular, compound **14** ($R_5$= F) was more active ($EC_{50}$= 4.0 ± 0.8 µM) than compound **13** ($EC_{50}$= 6.6 ± 0.2 µM), which has a chlorine atom at $R_5$. This difference in the antiviral activity could be explained by the greater electronegativity of the fluorine substituent. Finally, compound **15,** which presents a nitro group, a strong electron-withdrawing substituent, at position $R_5$, was the most active in the series of $N^4$-TSCs derived from 5,6-dimethoxy-1-indanone ($EC_{50}$= 0.7 ± 0.1 µM).

*3.4. BVDV-TSC$^r$ T1 cross-resistance studies*

Compounds **2** and **15** were evaluated against BVDV-TSC$^r$ T1, which carries two mutations (N264D and A392E) in the RdRp coding region (NS5B).[11] The CPE reduction assays revealed that BVDV-TSC$^r$ T1 was also resistant to compound **15** at the maximal concentration evaluated (10 µM) (Fig. 2C, Table 4) with an twenty-two fold increase in the $EC_{50}$ value when compared to the wild type virus ($EC_{50}$ > 10 µM and $EC_{50}$ = 0.45 ± 0.08 µM, respectively).

However, compound **2** showed inhibition of BVDV-TSC$^r$ T1 (Fig. 2B, Table 4), and no significant differences were observed between $EC_{50}$ values determined against the wild type virus and resistant virus.

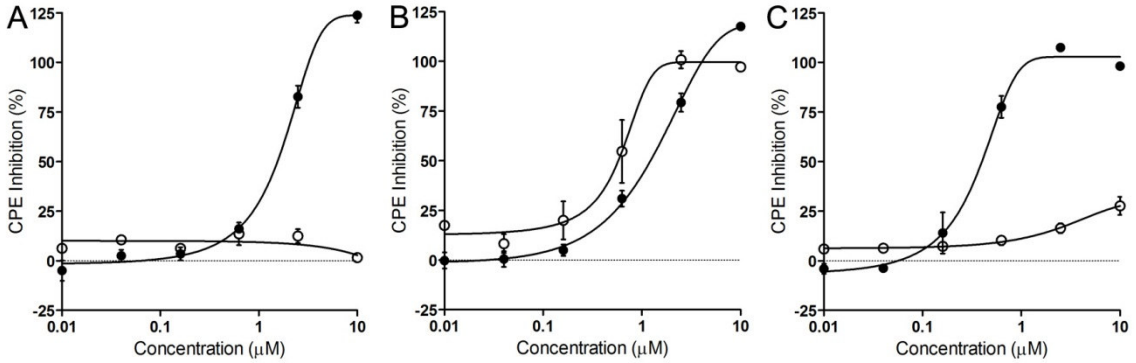


**Fig. 2**. *In vitro* antiviral activity of **5,6-TSC** (A), **2** (B) and **15** (C) against wild type and BVDV-TSC$^r$ T1. Representative dose-response curves from one of two independent experiments. Full circles: wild type BVDV; empty circles: BVDV-TSC$^r$ T1.

**Table 4.** Susceptibility of wt-BVDV and BVDV-TSC$^r$ T1 to active thiosemicarbazones.

| Viral Strain | NS5B mutations | $EC_{50}$ (μM) [a] | | |
|---|---|---|---|---|
| | | 5,6-TSC | Compound **2** | Compound **15** |
| Wild type BVDV | - | 1.95 ± 0.54 | 1.04 ± 0.39 | 0.45 ± 0.08 |
| BVDV- TSC$^r$ T1 | N264D, A392E | >80 (>41)[b] | 1.07 ± 0.69 | >10 (>22)[b] |

$EC_{50}$: compound concentration that reduces viral CPE by 50% with respect to the infected untreated control (UTC). [a]Data are mean values ± SD from at least two independent experiments. [b]The number between parentheses represents the calculated fold decrease in susceptibility of the resistant variant BVDV ($EC_{50}$ BVDV-TSC$^r$ T1 / $EC_{50}$ wt-BVDV).

*3.5. Time-of-drug-addition studies.*

In order to determine the time of the viral cycle at which compound **2** exerts its effects, time-of-drug-addition experiments were carried out. At different time points post- infection (p.i.), compound **2** at 25 µM was added. Viral replication was then evaluated as the CPE after 48 h of incubation (Fig. 3). Compound **2** showed the strongest inhibitory effect when it was added to the culture up to 4 h post-infection. Conversely, the addition of the compound at later time points resulted in a gradual loss of the antiviral activity. These data suggest that the drug may be exerting the effects after virus attachment and penetration but before virus assembly and release. Moreover, the time point at which compound **2** exerts its activity coincided with the onset of viral RNA synthesis (i.e., at about 6 h p.i.).[28]

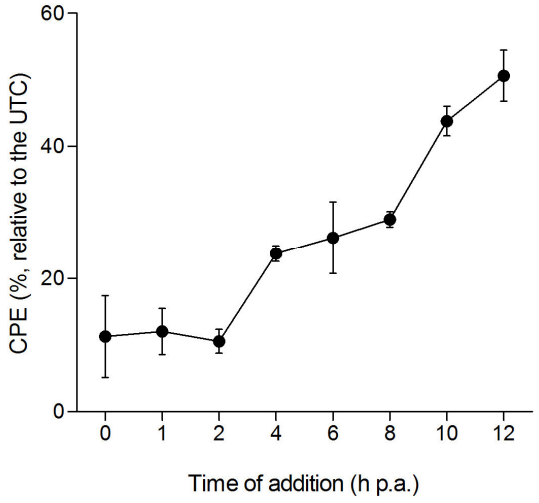


**Fig. 3**. Time-of-drug-addition study. MDBK cells were infected with BVDV (MOI=1), and compound **2** at 25 µM was added at different time points post-infection. After 48 h of incubation at 37 ºC, CPE was calculated from cell viability measures (MTS/PES method).

*3.6. Molecular docking study*

We have previously reported the interactions observed in the docking study performed between RdRp (PDB ID: 1S48) and 5,6-TSC close to N264 and A392, for both wild type and mutated (N264D and A392E) BVDV RdRp .[11] Herein, we explored the ligand-RdRp interactions for the most active compounds of the new set of derivatives (compounds **2**

and **15**) in order to better determine the preferred binding modes and the molecular requirements exploited by resistant mutants to escape drug inhibition.

The interaction between compound **15** and the wt-RdRp revealed (Fig. 4A): (i) two hydrogen bonds between the $N^2$ and the $N^4$ atoms of the thiosemicarbazone group and amino acids E226 and F224, respectively; (ii) a hydrogen bond between the oxygen of the 6-methoxy group and the hydroxyl group of Y289; (iii) a π-π stacking interaction between the aromatic ring attached to $N^4$ of the thiosemicarbazone moiety and the side chain of F224; (iv) a close contact between the indanic ring and A222. On the other hand, the situation in the best score pose of mutant RdRp-compound **15** complex (Fig. 4B) showed: (i) a hydrogen bond between the $N^1$ atom of the thiosemicarbazone group and the amino acid A222; (ii) a hydrogen bond between the $N^4$ of the thiosemicarbazone moiety and G220; (iii) a close contact between the indanic ring and A222; (iv) steric hindrance between the 5-methoxy group of the ligand and E392. For a further comparison between wild type and mutant complexes, we presented a second orientation of the ligand to the mutant RdRp which is similar to that adopted in the wild type RdRp (Fig. 4C). It was observed that despite the similar orientation of the ligand in the binding site, only one hydrogen bond is formed between $N^2$ of the thiosemicarbazone group and E226. Furthermore, it is noteworthy that no hydrogen bonds were formed between the 5,6-dimethoxy group of the indanic ring and the amino acids of the mutated enzyme. Therefore, it seems that the presence of this group plays a key role in the anti-BVDV activity. This observation is in line with the results obtained in the cross-resistance study. Moreover, $N^4$-TSCs lacking the 5,6-dimethoxy group in the indanic nucleus have no activity against BVDV.

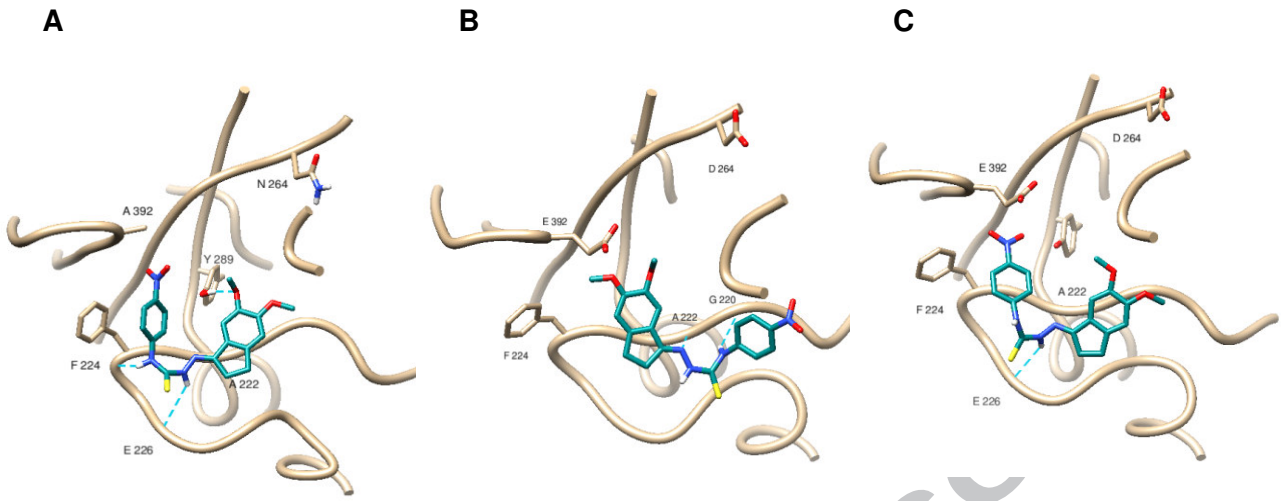


**Fig. 4**. Docking and binding pattern of compound **15** into BVDV RdRp (PDB ID: 1S48). $N^4$-TSC **15** is represented as a stick model according to atom types: carbons, cyan; nitrogens, blue; oxygens, red; sulphur, yellow; hydrogens, white. Cyan dashed lines indicate hydrogen bonds. The side chains making favorable interactions and those involved in resistant mutations are shown as stick models. (**A**) Details of the highest-score docked pose of **15** into the binding pocket of the wild type enzyme. (**B**) Details of the highest-score docked pose of **15** into the binding pocket of BVDV mutated RdRp. (**C**) Details of the docked pose of **15** with an orientation similar to that obtained for the wt-BVDV RdRp into the binding pocket of the mutated enzyme.

The interaction observed in the best score pose of wt-RdRp with compound **2** revealed (Fig. 5A): (i) a hydrogen bond established between the $N^4$ atom of the thiosemicarbazone group and amino acid P262; (ii) two hydrogen bonds between the oxygen atoms of the nitro group and amino acids A222 and G223; (iii) close contacts between the ring and the amino acids F224 and T259. The interaction between compound **2** and the mutated polymerase (Fig. 5B) showed: (i) a hydrogen bond between the $N^2$ atom of the thiosemicarbazone group and E392; (ii) two hydrogen bonds between the $N^4$ of the thiosemicarbazone moiety and E392 and P262; (iii) one hydrogen bond between the oxygen of the nitro group and A222. Although one more hydrogen bond was observed in

the resistant mutant RdRp compared to the wild type protein, the binding mode of the TSC **2** in the wild type form showed favorable close contacts that were absent in the mutated one. Accordingly, interactions appear to be largely maintained upon mutations. The latter finding is in agreement with the results obtained in the cross-resistance study.

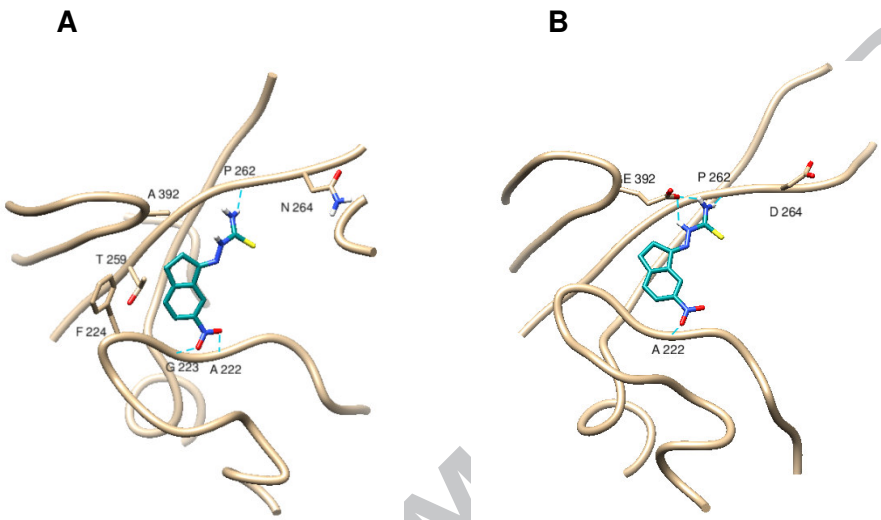


**Fig. 5**. Docking and binding pattern of compound **2** into BVDV RdRp (PDB ID: 1S48). TSC **2** is represented as a stick model according to atom types: carbons, cyan; nitrogens, blue; oxygens, red; sulphur, yellow; hydrogens, white. Cyan dashed lines indicate hydrogen bonds. The side chains making favorable interactions, and those involved in resistant mutations are shown as stick models. (**A**) Details of the highest-score docked pose of **2** into the binding pocket of the wild type enzyme. (**B**) Details of the highest-score docked pose of **2** into the binding pocket of mutated BVDV RdRp.

Finally, the preferred binding modes of 5,6-TSC and derivative **15** into wt-RdRp showed the same pattern of interactions, whereas a different pattern of interactions for compound **2** and the lead compound was observed (Fig. 6). These findings, taken together with the results obtained in the cross-resistance assay, would suggest that this binding site is not the molecular target for TSC **2**.

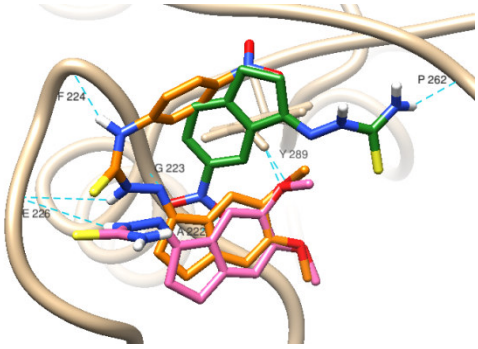


**Fig. 6.** Comparative docking and binding patterns of compounds 5,6-TSC, **2** and **15** into BVDV RdRp (PDB ID: 1S48). 5,6-TSC, **2** and **15** are represented as a stick model with carbons in pink, green and orange respectively. The other atom types are represented as follows: nitrogens, blue; oxygens, red; sulphur, yellow; hydrogens, white. Cyan dashed lines indicate hydrogen bonds.

*3.7. Binding free energy analysis*

The findings in the cross-resistant assay (Table 4) and the different binding poses of compounds **2** and **15** in the pocket of the viral polymerase (Fig. 4A, 5A and 6) raise the question of whether derivative **2** targets this binding site. Therefore, to further analyze the ligand-protein affinities we performed MM/PBSA calculations for the two derivatives in the wild type and N264D/A392E mutant enzyme. The calculated binding free energies are listed in Table 5.

**Table 5.** Binding free energies and its components for compounds **2** and **15** on wt-BVDV and BVDV-TSC$^r$ T1.

| | Compound **2** Wild type BVDV | Compound **2** BVDV- TSC$^r$ T1 | Compound **15** Wild type BVDV | Compound **15** BVDV- TSC$^r$ T1 |
|---|---|---|---|---|
| $\Delta E_{VDW}$ | -29.66 ± 0.10 | -28.71 ± 0.11 | -37.08 ± 0.12 | -35.69 ± 0.13 |
| $\Delta E_{ELE}$ | -10.47 ± 0.11 | -11.55 ± 0.13 | -14.12 ± 0.15 | -12.52 ± 0.17 |
| $\Delta G_{NP}$ | -3.74 ± 0.01 | -3.93 ± 0.01 | -4.07 ± 0.01 | -4.27 ± 0.01 |
| $\Delta G_{PB}$ | 26.89 ± 0.15 | 27.04 ± 0.14 | 32.82 ± 0.17 | 31.88 ± 0.18 |
| $-T\Delta S$ | 12.67 ± 0.75 | 12.71 ± 0.81 | 14.08 ± 0.81 | 14.03 ± 0.83 |
| $\Delta G_{bind}$ | -4.31 | -4.44 | -8.37 | -6.57 |

All energies are expressed in Kcal/mol. Data are mean values ± SD. $\Delta E_{VDW}$, van der Waals energy; $\Delta E_{ELE}$, electrostatic energy; $\Delta G_{NP}$, nonpolar solvation energy; $\Delta G_{PB}$, polar solvation energy; $-T\Delta S$, entropy contribution; $\Delta G_{bind}$, binding free energy.

As indicated in Table 5, derivative **15** complexed with wt-BVDV had the most favorable binding energy ($\Delta G_{bind}$ =-8.37) whereas the complex with the mutated enzyme caused a significative energetic change ($\Delta G_{bind}$ =-6.57). On the other hand, for ligand **2** both complexes displayed lower binding energies and, interestingly, with similar energies between them ($\Delta G_{bind}$=-4.31 and -4.44).

Comparisons of the free energies components were carried out to elucidate the interaction mechanism. In all complexes, the van der Waals energy was the most favorable interaction for binding, pointing out the major contribution of hydrophobic groups. Favorable interactions were also recorded in electrostatic energy and nonpolar solvation energy. However, they were counteracted by detrimental polar solvation energy and entropy. In addition, it should be noted that the inclusion of the entropic contribution did not change the order of the binding energies. It is evident that the van der Waals and electrostatic interactions were higher for derivative **15** complexed with the wild type

enzyme than that of other complexes. Thus, $\Delta E_{VDW}$ and then $\Delta E_{ELE}$ were the main driving forces involved in the binding of this inhibitor.

In summary, the values of $\Delta G_{bind}$ for compound **15** were in good agreement with the cross-resistance assay and provide more information regarding enzyme-ligand interactions in the selected pocket. In the case of compound **2,** results suggest a different binding site or target which may provide an explanation for the similar $EC_{50}$ values in the cross-resistance assay.

## 4. Conclusions

In the present study, a series of TSCs and $N^4$-arylsubstituted TSCs derived from 1-indanones was synthesized and evaluated as potential anti-BVDV agents. Six novel compounds were easily prepared by one-pot multicomponent reaction under microwave irradiation with good yields and short reaction times. The *in vitro* assays showed that two new derivatives (**2** and **15**) display enhanced activity compared to the lead compound 5,6-TSC. For $N^4$-TSCs, the structure-activity relationship study demonstrated that the 5,6-dimethoxy substitution of the indanic ring and $N^4$-aryl substitution of the thiosemicarbazone moiety arise as important structural features for antiviral activity as they mediate key ligand-protein interactions in the binding pocket on the viral polymerase. Moreover, the presence of electron-withdrawing substituents in the phenyl ring attached to $N^4$ atom of the thiosemicarbazone function increased the activity against BVDV. Cross-resistance assays combined with *in silico* studies showed that $N^4$-TSC **15** is highly likely to act as a non-nucleoside inhibitor of the viral polymerase. Further studies will be carried out to elucidate the mechanism of action of compound **2**. To conclude, derivatives **2** and **15** emerge as promising new lead compounds. The results obtained in the present work are of great relevance and provide valuable bases for further structural design in search for novel agents against BVDV.

**Acknowledgements**

We thank CONICET for scholarship to María C. Soraires Santacruz and Agencia Nacional de Promoción Científica y Tecnológica for scholarship to Matias Fabiani. This study was supported by the Universidad de Buenos Aires [UBACYT 2014–2017 200201130100005BA and 20020130100102BA], and by the Agencia Nacional de Promoción Científica y Tecnológica [PICT 2012-2867].

**References**

1. Houe H. Epidemiological features and economical importance of bovine virus diarrhoea virus (BVDV) infections. *Vet. Microbiol*. 1999; 64: 89–107.

2. Lindberg A, Brownlie J, Gunn GJ, Houe H, Moennig V, Saatkamp HW, Sandvik T, Valle PS. The control of bovine viral diarrhoea virus in Europe: today and in the future. *Rev. Sci. Tech*. 2006; 25: 961–979.

3. Presi P, Struchen R, Knight-Jones T, Scholl S, Heim D. Bovine viral diarrhea (BVD) eradication in Switzerland--experiences of the first two years. *Prev. Vet. Med*. 2011; 99: 112–121.

4. Pacheco JM, Lager I. Indirect method ELISA for the detection of antibodies against bovine diarrhea virus in bovine serum. *Rev. Argent. Microbiol*. 2003; 35: 19–23.

5. Al-Khaliyfa MA, Abuelzein EME, Gameel AA. Identification of cattle persistently infected with BVDV by ear-notch testing in Saudi Arabia. *Vet. Rec*. 2010; 167: 660–661.

6. González Altamiranda EA, Kaiser GG, Weber N, Leunda MR, Pecora A, Malacari DA, Morán O, Campero CM, Odeón AC. Clinical and reproductive consequences of using BVDV-contaminated semen in artificial insemination in a beef herd in Argentina. *Anim. Reprod. Sci*. 2012; 133: 146–152.

7. Bolin SR. Control of bovine viral diarrhea infection by use of vaccination. *Vet. Clin. North Am. Food Anim. Pract*. 1995; 11: 615–625.

8. Van Oirschot JT, Bruschke CJ, van Rijn PA. Vaccination of cattle against bovine viral diarrhoea. *Vet. Microbiol*. 1999; 64: 169–183.

9. Buckwold VE, Beer BE, Donis RO. Bovine viral diarrhea virus as a surrogate model of hepatitis C virus for the evaluation of antiviral agents. *Antiviral Res*. 2003; 60: 1–15.

10. Finkielsztein LM, Castro EF, Fabian LE, Moltrasio GY, Campos RH, Cavallaro LV, Moglioni AG. New 1-indanone thiosemicarbazone derivatives active against BVDV. *Eur. J. Med. Chem*. 2008; 43: 1767–1773.

11. Castro EF, Fabian LE, Caputto ME, Gagey D, Finkielsztein LM, Moltrasio GY, Moglioni AG, Campos RH, Cavallaro LV. Inhibition of bovine viral diarrhea virus RNA synthesis by thiosemicarbazone derived from 5,6-Dimethoxy-1-indanone. *J. Virol*. 2011; 85: 5436–5445.

12. Caputto ME, Fabian LE, Benítez D, Merlino A, Ríos N, Cerecetto H, Moltrasio GY, Moglioni AG, González M, Finkielsztein LM. Thiosemicarbazones derived from 1-indanones as new anti-Trypanosoma cruzi agents. *Bioorg. Med. Chem*. 2011; 19: 6818–6826.

13. Lansbury PT, Mancuso NR. Further studies of bond insertion and nonstereospecific Beckmann rearrangements in 7-alkyl-l-indanone oximes. *J. Amer. Chem. Soc*. 1966; 88: 1205–1212.

14. Morris GM, Huey R, Lindstrom W, Sanner MF, Belew RK, Goodsell DS, Olson AJ. AutoDock4 and AutoDockTools4: Automated docking with selective receptor flexibility. *J. Comput. Chem*. 2009; 30: 2785–2791.

15. Phillips JC, Braun R, Wang W, Gumbart J, Tajkhorshid E, Villa E, Chipot C, Skeel RD, Kalé L, Schulten K. Scalable molecular dynamics with NAMD. *J. Comput. Chem*. 2005; 26: 1781–1802.

16. Zhang Z, Li Y, Lin B, Schroeder M, Huang B. Identification of cavities on protein surface using multiple computational approaches for drug binding site prediction. *Bioinformatics*. 2011; 27: 2083–2088.

17. Pettersen EF, Goddard TD, Huang CC, Couch GS, Greenblatt DM, Meng EC, Ferrin TE. UCSF Chimera - A visualization system for exploratory research and analysis. *J. Comput. Chem*. 2004; 25: 1605–1612.

18. Best RB, Zhu X, Shim J, Lopes PEM, Mittal J, Feig M, Mackerell AD. Optimization of the additive CHARMM all-atom protein force field targeting improved sampling of the backbone ϕ, ψ and side-chain χ(1) and χ(2) dihedral angles. *J. Chem. Theory Comput.* 2012; 8: 3257–3273.

19. Vanommeslaeghe K, Hatcher E, Acharya C, Kundu S, Zhong S, Shim J, Darian E, Guvench O, Lopes P, Vorobyov I, MacKerell Jr. AD. CHARMM general force field: A force field for drug-like molecules compatible with the CHARMM all-atom additive biological force field. *J. Comput. Chem*. 2010; 31: 671–690.

20. Jorgensen WL, Chandrasekhar J, Madura JD. Comparison of simple potential functions for simulating liquid water. *J. Chem. Phys*. 1983; 79: 926–935

21. Darden T, York D, Pedersen L. Particle mesh Ewald: an N·log(N) method for Ewald sums in large systems. *J. Chem. Phys*. 1993; 98: 10089–10092.

22. Miyamoto S, Kollman PA. Settle: An analytical version of the SHAKE and RATTLE algorithm for rigid water models *J. Comput. Chem*. 1992; 13: 952–962.

23. Humphrey W, Dalke A, Schulten K. VMD - Visual Molecular Dynamics. *J. Molec. Graphics*. 1996; 14: 33–38.

24. Kollman PA, Massova I, Reyes C, Kuhn B, Huo S, Chong L, Lee M, Lee T, Duan Y, Wang W, Donini O, Cieplak P, Srinivasan J, Case DA, Cheatham TE 3rd. Calculating structures and free energies of complex molecules: combining molecular mechanics and continuum models. *Acc. Chem. Res.* 2000; 33: 889–897.

25. Tonelli M, Boido V, La Colla P, Loddo R, Posocco P, Paneni MS, Fermeglia M, Pricl S. Pharmacophore modeling, resistant mutant isolation, docking, and MM-PBSA analysis: combined experimental/computer-assisted approaches to identify new inhibitors of the bovine viral diarrhea virus (BVDV). *Bioorg. Med. Chem*. 2010; 18: 2304–2316.

26. Giliberti G, Ibba C, Marongiu E, Loddo R, Tonelli M, Boido V, Laurini E, Posocco P, Fermeglia M, Pricl S. Synergistic experimental/computational studies on arylazoenamine derivatives that target the bovine viral diarrhea virus RNA-dependent RNA polymerase. *Bioorg. Med. Chem*. 2010; 18: 6055–6068.

27. Carta A, Briguglio I, Piras S, Corona P, Ibba R, Laurini E, Fermeglia M, Pricl S, Desideri N, Atzori EM, La Colla P, Collu G, Delogu I, Loddo R. A combined in silico/in vitro approach unveils common molecular requirements for efficient BVDV RdRp binding of linear aromatic N-polycyclic systems. *Eur J Med Chem*. 2016; 117: 321–334.

28. Paeshuyse J, Chezal JM, Froeyen M, Leyssen P, Dutartre H, Vrancken R, Canard B, Letellier C, Li T, Mittendorfer H, Koenen F, Kerkhofs P, De Clercq E,Herdewijn P, Puerstinger G, Gueiffier A, Chavignon O, Teulade JC, Neyts J. The imidazopyrrolopyridine analogue AG110 is a novel, highly selective inhibitor of pestiviruses that targets the viral RNA-dependent RNA polymerase at a hot spot for inhibition of viral replication. *J Virol.* 2007; 20: 11046-11053

Highlights

- New $N^4$-arylthiosemicarbazones derived from 1-indanones were synthesized
- Two thiosemicarbazones were identified as potent inhibitors of BVDV replication
- Structural features related to the anti-BVDV activity were identified
- Cross-resistance assays were performed to investigate the molecular target
- Molecular docking between most active compounds and viral polymerase are reported